ACS OMEGA

http://pubs.acs.org/journal/acsodf

Article

Electronic and Optical Properties of $CsGeX_3$ (X= Cl, Br, and I) Compounds

Nguyen Thi Han, Vo Khuong Dien,* and Ming-Fa Lin*

Cite This: *ACS Omega* 2022, 7, 25210−25218

Read Online

ACCESS | Metrics & More | Article Recommendations | Supporting Information

ABSTRACT: We used first-principles calculations to investigate the electrical and optical properties of $CsGeX_3$ (X = Cl, Br, and I) compounds. These materials present rich and unique physical and chemical phenomena, such as the optimal geometric structure, the electronic band structure, the charge density distribution, and the special van Hove singularities in the electronic density of states. The optical properties cover a slight red shift of the optical gap, corresponding to weak electron−hole interactions, strong absorption coefficients, and weak reflectance spectra. The presented theoretical framework will provide a full understanding of the various phenomena and promising applications for solar cells and other electro-optic materials.

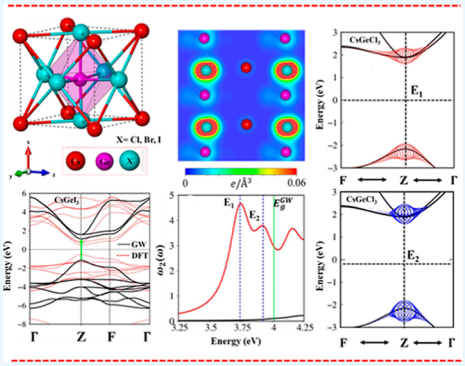

1. INTRODUCTION

Nowadays, solar cell devices have become one of the outstanding systems in engineering applications and basic science research studies[1−4] because they can provide eco-friendly and renewable energy and are efficient by using a special route to convert photon energy into electricity.[5−13] The principal architectures of the perovskite solar cell include the absorber layer sandwich between the electron-transporting and hole-transporting layers, in which the first component is very important since it absorbs the electromagnetic wave and generates the electron−hole pairs. Apparently, the geometric, electronic, and optical features of these components are regarded as very important characteristics. These factors should be critical in determining the efficiency of light-generated currents and finding the best combination of the three kinds of core components.

Up to now, inorganic perovskite materials,[14−16] such as $CsPbX_3$ (X = Cl, Br, and I),[17,18] have attracted more and more research attention for energy harvesting applications due to their excellent photoelectronic properties. However, there are still many disadvantages,[17] for example, the limit of large-scale applications owing to the toxicity of the lead element.[19] Currently, the lead-free $CsGeX_3$ (X = Cl, Br, and I) compounds are other candidates to replace $CsPbX_3$ perovskites for solar cell and other applications.[19,20] In fact, such compounds cover many interesting properties/novel features and have been investigated by both previous theoretical[21−28] and experimental methods.[29−32]

On the experimental side, Li et al. have successfully synthesized the $CsGeI_3$ compound and demonstrated that this material processes a high photocurrent (6 mA cm^2), which means that it is suitable for photovoltaic applications.[29] To enhance the photocurrent generation of WS_2 nanoflakes, WS_2/$CsGeBr_3$ has been fabricated, with an external quantum yield and a responsivity of about ∼151% and 6.4 (A/W), respectively.[30] The absorption edges of $CsGeCl_3$ and $CsGeBr_3$ are very sensitive and significantly red-shift under applied external hydrostatic pressure. This phenomenon was verified by the experiment of Schwarz and his co-workers.[31] Besides, photoluminescence and absorption measurements of $CsGeCl_3$, $CsGeBr_3$, and $CsGeI_3$ have been reported.[32]

On the theoretical aspects, the fundamental electrical and optical properties of the $CsGeCl_3$, $CsGeBr_3$, and $CsGeI_3$ materials have been investigated with various approaches, such as first-principles calculations,[26,33] the effective mass approximation,[33] and the tight-binding model;[23,34] among them, the first-principles calculations are the most effective approach to identify the optimal geometric, electronic, and optical properties of these compounds. According to current theoretical predictions, $CsGeX_3$ belongs to the direct gap semiconductor materials,[21] with their gap values ranging from 0.82 to 7.91 eV, depending on the approximations.[22−27] For example, using the Perdew−Burke−Ernzerhof (PBE)-sol functional, Jong et al.[33] provided the energy band gaps of 1.19, 1.46, and 2.13 eV[28] for $CsGeI_3$, $CsGeBr_3$, and $CsGeCl_3$,

Received: April 4, 2022
Accepted: June 29, 2022
Published: July 13, 2022

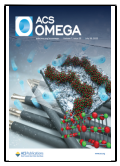

respectively. The accuracy of the energy gap could be improved with the typical values of 1.64, 2.34, and 3.24 eV for $CsGeI_3$, $CsGeBr_3$, and $CsGeCl_3$, respectively, when adopting the hybrid functional (HSE) approximation.

Generally, the geometric and electronic properties of $CsGeX_3$ have been studied; however, the critical factors, such as the orbital hybridizations[35] in the chemical bonds, have not been discussed in detail. Only a few studies have been performed on the optical properties so far;[20,26,33,36] most theoretical investigations are based on the density functional theory (DFT), and thus, the theoretical predictions on optical properties of $CsGeX_3$ compounds do not accommodate the experiment results.[32] Note that the operation of a solar cell is highly dependent on the formation of excitons since the charge separations are hugely influenced by these electron−hole bound states. Although the excitonic effects in the broad energy range of materials,[33,37] including $CsGeX_3$,[33] have been qualitatively estimated by effective mass models, the quantitative description of these bound states is rather limited. There are few works that relied on ab initio Bethe−Salpeter equation (BSE) calculations;[20,38−40] however, the formation as well as the nature of the excitonic states has not been elucidated yet.

In this work, the first-principles calculations were utilized to investigate the geometric and electronic properties and effects of the electron−hole interactions on the optical properties of the $CsGeX_3$ (X = Cl, Br, and I) compounds. The theoretical framework is based on the examination of the geometric structure, the accurate quasi-particle energy band structure, the special van Hove singularities on the electronic density of states (DOS), the band decomposed charge densities, the dielectric functions in the case of presence/absence of excitonic effects, the exciton wave functions, and other related optical properties. As a result, the influences of excitonic effects on the optical absorption spectrum and its nature have been clarified. The $CsGeCl_3$, $CsGeBr_3$, and $CsGeI_3$ compounds are excellent candidates for solar cell and opto-electronic applications. The presented theoretical studies in this work are useful for solar cells and other materials.

2. COMPUTATIONAL DETAILS

We investigated the DFT based on the VASP Package[41] to present the optimized structure of the $CsGeCl_3$, $CsGeBr_3$, and $CsGeI_3$ compounds. The related problems to exchange−correlation functions were solved by adopting the PBE form of the generalized gradient approximation (GGA).[42] To treat the core issues, the projector augmented wave (PAW) pseudopotential was used.[43] The cutoff energy of 500 eV was used for the expansion of the plane wave. The Brillouin zone was integrated with a sufficient k-point mesh of 20 × 20 × 20 in the Γ-centered sampling technique for optimizing the geometric structure. Between two successive simulation steps, the ground state's convergence condition was set to 10^{-8} eV. During the geometric optimization, all atoms and the cell could fully relax until the Hellmann−Feynman force acting on each atom was smaller than 0.01 eV.[28,44]

In the current research, the electronic properties of $CsGeCl_3$, $CsGeBr_3$, and $CsGeI_3$[45,46] were studied by using the GW method (G stands for Green's function and W represents the screened Coulomb potential), in which the quasi-particle energies were obtained within the G3W0 approximation (three self-consistent updates for the quasi-particle Green's function) for the self-energy,[47] the response function's cutoff energy was set to 200 eV, and 12 × 12 × 12-centered k-points sampling was used to represent reciprocal space. The quasi-particle band structure was plotted by using the Wannier 90 code.[48,49] Simultaneously, the DFT electronic band structures in the case of with/without spin−orbit coupling (SOC) are also calculated for comparison. However, the SOC effects have been ignored in our GW calculations due to the extremely expensive many-body effects. Based on the electronic wave functions, the single-particle excitations were described by Fermi's golden rule[50]

$$\epsilon_2(\omega) = \frac{8\pi^2 e^2}{\omega^2} \sum_{vc\boldsymbol{k}} |e\langle v\boldsymbol{k}|\boldsymbol{v}|c\boldsymbol{k}\rangle|^2 \delta(\omega - (E_{c\boldsymbol{k}} - E_{v\boldsymbol{k}}));$$

in which the intensity of the excitation peaks is described by the matrix element, $|e\langle v\boldsymbol{k}|\boldsymbol{v}|c\boldsymbol{k}\rangle|^2$, while the available transition channels are defined by the joined DOS, $\delta(\omega - (E_{c\boldsymbol{k}} - E_{v\boldsymbol{k}}))$.

In addition to the independent particle excitations, the presence of exciton states may have a significant impact on the optical responses. The wave functions related to these bound states of electrons and holes could be expressed by using the following expression

$$|S\rangle = \sum_{\boldsymbol{k}s} \sum_{v}^{\text{hole}} \sum_{c}^{\text{elec}} A^s_{vc\boldsymbol{k}} |vc\boldsymbol{k}\rangle;$$

in which the amplitude $A^s_{vc\boldsymbol{k}}$ is determined by solving the standard BSE[51]

$$(E^{\text{QP}}_{c\boldsymbol{k}} - E^{\text{QP}}_{v\boldsymbol{k}}) A^s_{vc\boldsymbol{k}} + \sum_{v'c'\boldsymbol{k}'} \langle vc\boldsymbol{k}|K^{\text{eh}}|v'c'\boldsymbol{k}'\rangle A^s_{vc\boldsymbol{k}} = \Omega^s A^S_{vc\boldsymbol{k}},$$

where $E^{\text{QP}}_{c\boldsymbol{k}}$ and $E^{\text{QP}}_{v\boldsymbol{k}}$, respectively, are the quasi-particle energies of the valence and the conduction states as obtained with the GW method. K^{eh} is the kernel describing the correlated electron−hole pairs, and $\Omega^s$is the energy of the excited states. The imaginary part of the dielectric function $\epsilon_2(\omega)$ is calculated from the excitonic states as

$$\epsilon_2(\omega) \propto \sum_S \left| \sum_{cv\boldsymbol{k}} A^s_{vc\boldsymbol{k}} \langle v\boldsymbol{k}|\boldsymbol{v}|c\boldsymbol{k}\rangle \right|^2 \delta(\omega - \Omega^s).$$

In this part, the Tamm−Dancoff approximation[52] was used; moreover, the energy cutoff and k-point sampling are set resemblances as in the GW calculations. Lorentzian with 100 meV broadening was used to replace the delta function. Since we are dealing with the low-frequency part of the absorption spectra, the four lowest conduction bands (CBs) and the seven highest valence bands (VBs) in the Bethe−Salpeter kernel are sufficient to describe the excitonic effects. All parameters in this works have carefully tested for the convergence of the calculations (Figure 1).

3. RESULTS AND DISCUSSION

The primitive cell of inorganic $CsGeX_3$ (X = Cl, Br, and I) perovskite materials is depicted in Figure 2a. These structures are part of the $R3m$ space group. A unit cell consists of one Cs atom, one Ge atom, and three Cl/Br/I atoms. The optimized lattice parameters have been calculated and are shown in Table 1 after achieving full lattice and atomic relaxations, the minimum of total energy. The calculated lattice constants of the these compounds agree with the available experimental and theoretical results.[26,28] The basic architecture of $CsGeX_3$ includes the Cs atom with a preferred 12 Cl/Br/I atom

https://doi.org/10.1021/acsomega.2c02088
ACS Omega 2022, 7, 25210−25218

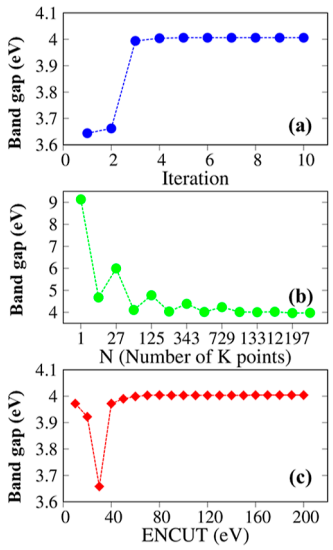

Figure 1. Convergence of the electronic band gap of $CsGeCl_3$ with respect to (a) self-consistent updates, (b) *k*-grid, and (c) cutoff frequency.

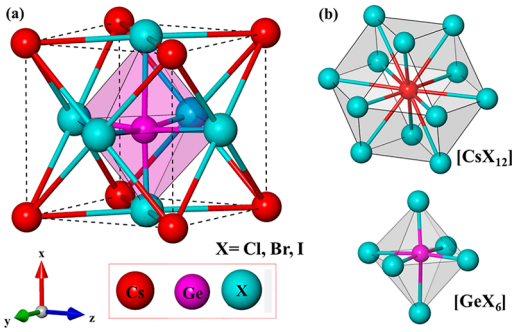

Figure 2. (a) Geometric structure of $CsGeX_3$; the unit cell is dashed black. (b) Two kinds of chemical bondings: $[CsX_{12}]$ and $[GeX_6]$ (X = Cl, Br, and I).

coordinate number, and the Ge atom is centered in the slightly distorted octahedron with three different Ge−Cl/Ge−Br/Ge−I chemical bonds (Figure 2b). This type of octahedral distortion causes electric polarization which occurs spontaneously, which can improve the separation of charge carriers and allow the photovoltage to exceed the band gap.[53,54] Furthermore, the slightly non-uniform environment demonstrates the rather complex hybridizations of orbitals in the chemical bonds, which are responsible for the essential electronic and optical properties.

The $CsGeX_3$ perovskite compounds sketch unique electronic properties which are entirely reflected in the energy band structure along the high symmetry points in the first Brillouin zone, named **Γ−*Z*−*F*−Γ**. The effective energy which is related to the main electronic features of these compounds lies mostly in the energy range of −8.0−6.0 eV (left panel in Figure 3). Obviously, a lot of sub-bands are formed by specific atoms with numerous orbitals in the unit cell. The energy dispersions of these states reveal the parabolic, saddle, and camelback shapes (−5 to −2 eV). Many maximum and minimum points in the wave-vector space generate van Hove singularities in the DOS. The $CsGeX_3$ compounds belong to direct band gap semiconductors, in which the lowest unoccupied states and the highest occupied ones locate on

Table 1. Number of Bonds, the Bond Length of Chemical Bonding of Cs−Cl/Cs−Br/Cs−I and Ge−Cl/Ge−Br/Ge−I Bonds, and the Lattice Constant of the $CsGeX_3$ (X = Cl, Br and I) Compounds

				lattice constant	
space group (*R*3*m*)	atom−atom	number of bonds	bond length (Å)	*a* (Å)	*α* (deg)
$CsGeCl_3$	Cs−Cl	12	3.90,3.91, 3.97	5.53	89.66
				5.33[a]	89.88[a]
	Ge−Cl	6	2.41,3.14	5.53[b]	88.98[b]
				5.44[c]	89.63[c]
$CsGeBr_3$	Cs−Br	12	4.03,4.09, 4.17	5.77	88.61
				5.56[a]	89.15[a]
	Ge−Br	6	2.58,3.21	5.78[b]	88.35[b]
				5.63[c]	88.74[c]
$CsGeI_3$	Cs−I	12	4.30,4.40	6.10	88.61
				5.94[a]	88.68[a]
	Ge−I	6	2.79,3.30	6.15[b]	87.78[b]
				5.98[c]	88.61[c]

[a]The lattice parameters were determined from the PBE functional from ref 33 [b]The lattice parameters were determined from the PBE functional from ref 20 [c]These values are from experiments.[60]

the same *Z* point. The effects of SOC make a minor reduction of the gap; these effects are significantly smaller than that of $CsSnX_3$[34] or $CsPbX_3$[34,55] due to the lighter Ge atom. In addition, the relativity effects also cannot create the higher spin degeneracy breaking in the electronic state vicinity of the Fermi level, and thus, the dark excitons due to spin-forbidden transitions are totally absent. The gap values of the DFT calculations in the absence and presence of SOC are summarized in Table 2 and Figure S1 (Supporting Information), and these results are in accordance with previous works.[16−18] After the *GW* approximations are adopted, the band gap values are increased to 4.01, 3.05, and 1.88 eV, respectively, for $CsGeCl_3$, $CsGeBr_3$, and $CsGeI_3$ compounds. The slightly over-estimated band gap values originate from the absence of SOC.

The effective mass of the hole/electron, being inversely proportional to the second-order derivative of energy, is able to reveal the carrier mobility. Since the carrier mobility in most cases is not strongly dependent on the band gap and the *GW* corrections insignificantly modify the band curvatures, for simplicity, we evaluate the effective mass at the DFT level of theory. According to delicate analysis, we can evidence that the hole states in the top of the VB are faster than the electron ones in the bottom of the CB for all $CsGeX_3$ compounds. Additionally, we can also see that the effective mass/kinetic energy decreases/increases as the halogen changes from Cl and Br to I (Table 3). This behavior is related to the interactions between the nuclear charge and valence charge of the halogen atoms. In fact, the interactions of valence charge in the halogen atoms with its nuclear charge decrease in the following order: Cl > Br > I atom. The weaker interaction of the latter mostly comes from the larger atomic radius, and thus, its carriers are less tightly bound to the nuclei/higher mobility than the formers. The electronic band structure, the carrier mobility, and projected DOS together with the band decomposed charge density can be used to fully understand the origination and behavior of excitons in the $CsGeX_3$ compounds.

https://doi.org/10.1021/acsomega.2c02088
ACS Omega 2022, 7, 25210−25218

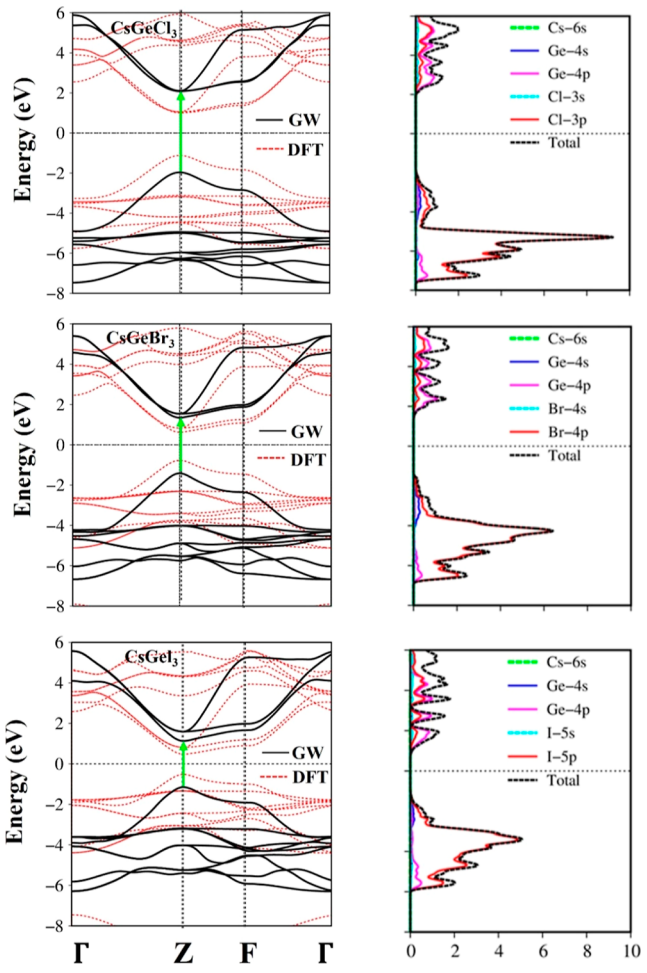

Figure 3. Left panels show the *GW* quasi-particle band structures of the $CsGeCl_3$, $CsGeBr_3$, and $CsGeI_3$ compounds (solid black). The green arrows at the *Z* point indicate the direct gaps. In addition, DFT electronic band structures are also added for comparisons (dash red). Right panels indicate the van Hove singularities in the DOS of $CsGeCl_3$, $CsGeBr_3$, and $CsGeI_3$ compounds.

In addition to quasi-particle energy band structures, the DOS could provide complete information about the electronic properties as well as the orbital hybridizations in the chemical bonds. As clearly indicated in the right panels in Figure 3, the DOS of three-dimensional $CsGeX_3$ compounds exhibits a lot of symmetric/asymmetric and shoulder structures arising from the parabolic, saddle, and dispersionless energy sub-bands in the band structure. The van Hove singularities of different orbitals mixed with each other are evidence of the complicated orbital hybridizations in the chemical bonds. Around the Fermi level, the DOS disappears and creates a sizable energy band gap of 4.01, 3.05, and 1.88 eV for $CsGeCl_3$, $CsGeBr_3$, and $CsGeI_3$, respectively. According to the orbital-projected DOS, the occupied states around the Fermi level can be divided into three paths, for example, for $CsGeCl_3$, (i) -8 eV $< E^v < -5$ eV is due to the strong orbital hybridizations of Ge-4p and Cl-3p states and (ii) -5 eV $< E^v < -2$ eV is co-dominated by the Ge-4s and Cl-3p orbitals. Apparently, due to the very high ionization energy, the contributions of the Cl-3s orbital lie very deep and thus do not hybridize with the others. As for the $CsGeBr_3$ and $CsGeI_3$ cases, these states move farther up, reflecting the higher atomic energy levels in the latter elements of the periodic table. For the unoccupied states, (iii) 2 eV $< E^c <$ 6 eV is mainly dominated by Cl-3p and Ge-4p orbitals and only has slight contributions to the Cs-6s states. Similar phenomena are also observed for the $CsGeBr_3$ and $CsGeI_3$ compounds. The relationship between the energy band structures, the projected DOS, and the band decomposed charge densities (discussed later) can identify the orbital hybridizations in all Cs−Cl/Cs−Br/Cs−I and Ge−Cl/Ge−Br/Ge−I bonds of the 3D $CsGeCl_3$, $CsGeBr_3$, and $CsGeI_3$ compounds, respectively.

To further comprehend the orbital hybridizations of the Cs−Cl/Cs−Br/Cs−I and Ge−Cl/Ge−Br/Ge−I chemical bonds, we have constructed the band decomposed charge densities (Figure 4a−c) for three parts of the valence and conduction states for the $CsGeCl_3$, $CsGeBr_3$, and $CsGeI_3$ compounds. Since the plots for the $CsGeCl_3$ compound look so similar to those of $CsGeBr_3$ and $CsGeI_3$, we only present the figures for $CsGeCl_3$ as an example. As seen in Figure 4a, the lower portion of the occupied states (-8 eV $< E^v < -5$ eV) clearly presents the π bonding character of the Ge-4p and Cl-3p orbitals, in which the Cl-3p charge density exhibits an important contribution. The charge density on the top of the

Table 2. Electronic Properties of $CsGeX_3$ Compounds: Fundamental Electronic Band Gap from DFT, DFT + SOC, HSE, HSE + SOC, and *GW* Approximations[a]

	band gap (eV)					
systems	DFT	DFT + SOC	HSE	HSE + SOC	*GW*	EX
$CsGeCl_3$	2.12	2.05	2.81	2.28[b]	4.01	3.40[d]
	2.13[b]	2.08[b]	3.24[b]		4.37[c]	
	2.07[c]	2.01[c]				
	1.97[c]					
$CsGeBr_3$	1.40	1.35	1.98	1.77[b]	3.05	2.39[d]
	1.46[b]	1.42[b]	2.34[b]		2.69[c]	
	1.44[c]	1.39[c]				
	1.09[d]					
$CsGeI_3$	1.05	0.88	1.44	1.52[b]	1.88	1.63[e]
	1.19[b]	1.06[b]	1.64[b]		1.69[c]	
	1.14[c]	0.99[c]				
	0.80[d]					

[a]The experimental (EX) results are also listed for comparison. [b]The electronic band gap estimated from ref 33 [c]The electronic band gap estimated from ref 20 [d]These values are from experiments.[20] [e]Reference.[61]

https://doi.org/10.1021/acsomega.2c02088
ACS Omega 2022, 7, 25210−25218

Table 3. Effective Mass of Electrons, Holes, and Reduced Mass Calculated with the PBE Functional[a]

systems	m_e^*	m_h^*	μ	$\varepsilon_1(0)$ DFT	$\varepsilon_1(0)$ *GW*	$\varepsilon_1(0)$ *GW* + BSE	E_b(eV)
$CsGeCl_3$	0.272	0.284	0.139	3.36	1.70	2.45	0.28
	0.450[b]	0.300[b]	0.140[c]	3.24[b]			
	0.270[c]	0.280[c]					
$CsGeBr_3$	0.176	0.181	0.089	4.29	1.97	2.85	0.25
	0.191[b]	0.197[b]	0.09[c]	3.88[b]			
	0.180[c]	0.190[c]					
$CsGeI_3$	0.137	0.143	0.070	5.86	2.53	4.19	0.14
	0.176[b]	0.186[b]	0.080[c]	4.83[b]			
	0.150[c]	0.160[c]					

[a]The static dielectric constants of with and without excitonic effects and exciton binding energy calculated from the *GW* + BSE method. [b]The effective mass of electrons and holes was calculated with the DFT method.[61] [c]Referene.[33]

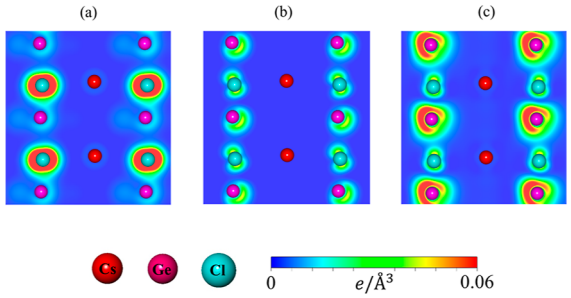

Figure 4. Band decomposed charge densities of $CsGeCl_3$: (a) lower portion of VBs (-8 eV < E^v < -5 eV), (b) upper portion of the VBs (-5 eV < E^v < -2 eV), and (c) bottom portion of the CBs (2 eV < E^c < 6 eV).

VBs (-5 eV < E^v < -2 eV) (Figure 4b) is dominated by σ bonding states formed from the comparable contribution of the Cl-3p and Ge-4s states. On the other hand, the lower portion of the unoccupied states (2 eV < E^c < 6 eV) (Figure 4c) clearly shows the σ bonding behavior originating from Cl-3p and Ge-4p states. The Ge states in this portion have a somewhat higher density than those on the top of the VBs because of the large contribution of Ge-4p orbitals. For the entire energy spectrum, the charge density associated with the Cs element is insignificant since it is related only to the 6s orbital. The band decomposed charge density, together with the energy band structure and the partial charge DOS, is useful for comprehending the orbital characters of the exciton states in the optical properties.

To understand the optical properties, the real part [$\varepsilon_1(\omega)$] and imaginary part [$\varepsilon_2(\omega)$] of the dielectric functions in the absence/presence of the excitonic effects of the $CsGeX_3$ systems were investigated (Figure 5). In the absence of hole and electron couplings, the real part of the dielectric function $\varepsilon_1(\omega)$ is weakly dependent on the energy in the inactive region, and the dielectric constant at zero energy $\varepsilon_1(0)$ is about 1.7, 2.0, and 2.7 eV, respectively, for the $CsGeCl_3$, $CsGeBr_3$, and $CsGeI_3$ compounds. These values increase after the excitonic effects have been adopted (details in Table 3). The ordering of the dielectric constant of $CsGeX_3$ is satisfied with its band gap values and strongly affects the exciton binding (discussed later). Moreover, the dispersionless feature of the real part at the low frequency is also an important factor to determine the vanishing range of the absorption coefficients $\alpha(\omega)$ and the reflectance coefficient $R(\omega)$ in the low energy region.

Concerning the imaginary part, $\varepsilon_2(\omega)$, the optical gap (green color) is about 4.00, 3.03, and 1.89 eV, respectively, for the $CsGeCl_3$, $CsGeBr_3$, and $CsGeI_3$ compounds in the absence of the excitonic effects. These values are equal to the fundamental direct gap E_g^i in Figure 3 owing to the conservation of the momentum. After taking into account the Coulomb interactions, the excitation strength is enhanced due to the enhancement of the electron–hole wave function overlap. Moreover, the presence of the excitonic effects also creates a slightly red-shifted threshold energy. The exciton binding is defined as the difference between the fundamental band gap and the optical gap after taking the Coulomb interaction into account; furthermore, the binding energy is also strongly proportional/inversely proportional to the effective mass of the carriers/dielectric screening constants. According to the delicate analysis, the typical exciton binding energy of $CsGeX_3$ lies in the following order: Cl > Br > I atom (Table 3 and Figure 5g–i); this trend agrees well with the effective mass model.[33,56] It is very important to note that the electron–hole interactions in $CsGeI_3$ are relatively weak and comparable with those in the $CsPbI_3$ solar cell;[55] the meta-stable exciton states easily break down to create free electron and hole carriers and thus efficiently generate the electrical currents.

Apparently, the first two peaks (E_1 and E_2) in Figure 6 are due to the excitonic effects since the excitation spectra without Coulomb attraction interactions nearly disappear in the ranges of 0 to 4 eV, 0 to 3 eV, and 0 to 2 eV for the $CsGeCl_3$, $CsGeBr_3$, and $CsGeI_3$ compounds, respectively. These sharp peaks originated from the coherent superposition of exciting electrons and holes. According to the exciton wave functions, as clearly depicted, the exciton states are located in the reciprocal space. Going from chlorine to iodine, the effective mass of carriers and the band gap decreases, and as a consequence, the extent of the exciton in *k*-space decreases. The first and second exciton states, respectively, arise from the vertical transitions from the last valence states to the first and second conduction states of the band extreme in the vicinity of the *Z* points (the blue and red circles in Figure 6), in which the excited holes and the excited electrons are characteristic for the Ge-4s, Cl-3p/Br-4p/I-5p, and Ge-4p orbitals, respectively. Obviously, owing to the high excitation strength around the visible region and beyond, the unique optical excitations of the $CsGeCl_3$, and $CsGeBr_3$ compounds can be used for electro-optics applications; specially, the $CsGeI_3$ compound can be exploited for photovoltaic applications.

The absorption coefficient $\alpha(\omega)$,[57] the imaginary part of the refractive index $k(\omega)$, the real part of the refractive index[58]

https://doi.org/10.1021/acsomega.2c02088
ACS Omega 2022, 7, 25210–25218

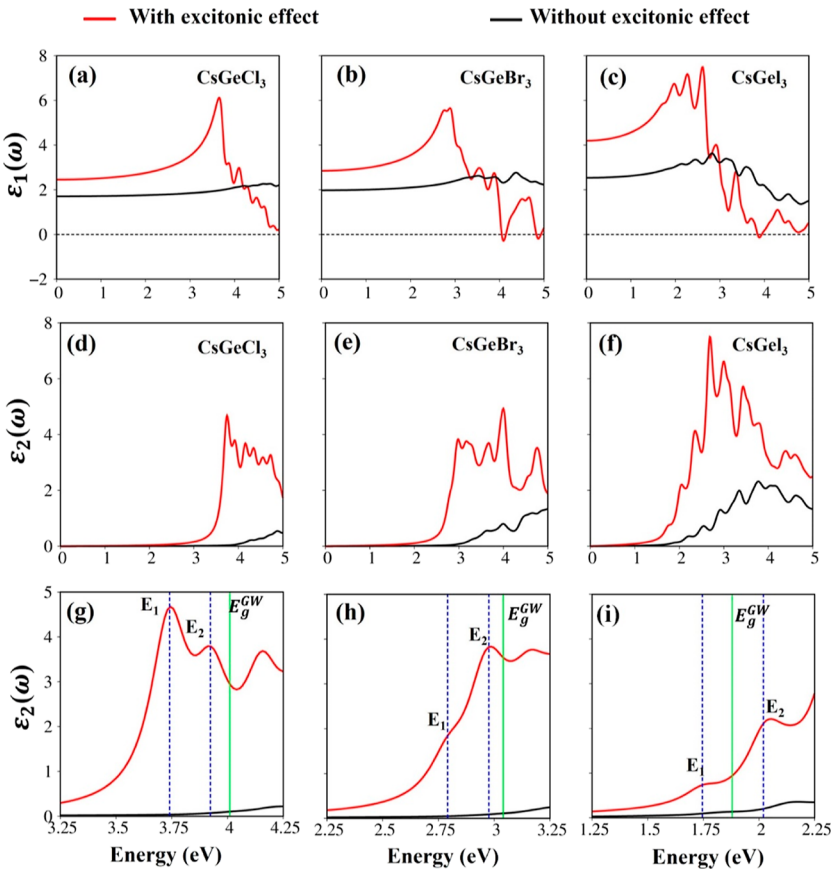

Figure 5. (a–c) Real part $\varepsilon_1(\omega)$ and (d–f) the imaginary part $\varepsilon_2(\omega)$ of the dielectric functions with/without excitonic effects for the $CsGeCl_3$, $CsGeBr_3$, and $CsGeI_3$ compounds, respectively. (g–i) Enlarged figures for the imaginary part $\varepsilon_2(\omega)$ of the dielectric functions for the $CsGeCl_3$, $CsGeBr_3$, and $CsGeI_3$ compounds, respectively. The dash-blue line represents E_1 and E_2 exciton peaks, and the green line indicates the fundamental gap.

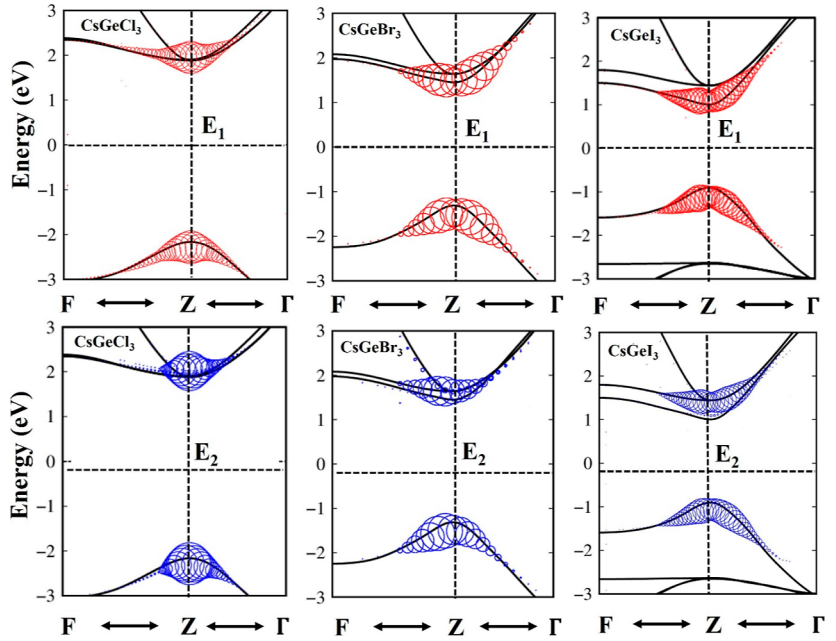

Figure 6. Exciton wave functions of the $CsGeCl_3/CsGeBr_3/CsGeI_3$ compound are predicted as fat-band pictures. The red and blue circles show two E_1 and E_2 exciton peaks in the imaginary part of the dielectric functions, respectively.

$n(\omega)$, and the reflectivity $R(\omega)$[59] have been calculated and are shown in Figure 7a–c to better elucidate the optical properties of the $CsGeCl_3$, $CsGeBr_3$, and $CsGeI_3$ compounds. Apparently, these compounds reveal strong absorption and weak reflectance coefficients. The $\alpha(\omega)$ is equal to 0, and the $R(\omega)$ is almost independent of the energy in the visible region

https://doi.org/10.1021/acsomega.2c02088
ACS Omega 2022, 7, 25210−25218

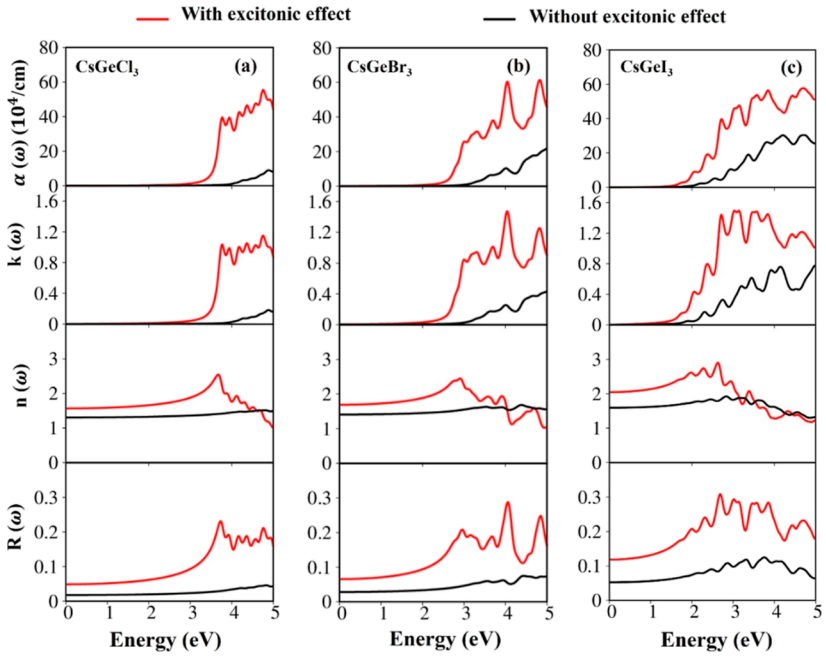

Figure 7. Absorption coefficient $\alpha(\omega)$, the imaginary part of the refractive index $k(\omega)$, the real part of the refractive index $n(\omega)$, and the reflectivity $R(\omega)$ for the $CsGeCl_3$ (a), $CsGeBr_3$, (b) and $CsGeI_3$ (c) compounds with and without excitonic effects.

as they lack electronic excitation contributions. The fast increase of the absorption coefficient is contributed by the various inter-band transitions. The inverse values of the absorption coefficient are equal to 400, 200, and 100 Å for $CsGeCl_3$, $CsGeBr_3$, and $CsGeI_3$, respectively. These findings imply that photons propagating in the medium are easily absorbed by the rich electronic excitations. As for the reflectance coefficient, the static reflective index is $R(0)$ is $\sim \left|\frac{\sqrt{\varepsilon_1(0)}-1}{\sqrt{\varepsilon_1(0)}+1}\right|^2$ = 0.05, 0.08, and 0.13 eV for the $CsGeCl_3$, $CsGeBr_3$, and $CsGeI_3$ compounds, respectively. A significant enhancement and a huge fluctuation are presented at a higher frequency. Obviously, these materials reveal low reflectivity and strong absorption, making them excellent candidates for solar cell applications.

4. CONCLUSION AND REMARKS

To summarize, accurate first-principles calculations were performed to calculate the rich and unique electronic and optical properties of $CsGeX_3$ (X = Cl, Br, and I) compounds. Consequently, the essential properties and potential applications for solar cell materials can be fully comprehended. The featured characteristics of these materials include an unusual geometric structure, unique electronic properties with a direct electronic band gap nature, the complicated orbital hybridizations comprehended from the electronic band structure, the band decomposed charge density, and the special van Hove singularities in the DOS. In addition, the exciton states and their nature have been qualitatively and quantitatively evaluated through delicate analysis on the mobility of carriers, the dielectric screening, orbital hybridizations in the initial and final states, and the exciton wave functions; other optical properties such as reflectance spectra and absorption coefficient are also achieved. Most importantly, the exciton binding of these materials is reliable to allow for the production of an electrical current upon sunlight adsorption. As a result, $CsGeX_3$ (X = Cl, Br, and I) compounds emerge as promising candidates for solar cell and electro-optics applications.

■ ASSOCIATED CONTENT

Supporting Information

The Supporting Information is available free of charge at https://pubs.acs.org/doi/10.1021/acsomega.2c02088.

Calculation results of the band structures by DFT and DFT + SOC corresponding to $CsGeCl_3$, $CsGeBr_3$, and $CsGeI_3$ compounds (PDF)

■ AUTHOR INFORMATION

Corresponding Authors

Vo Khuong Dien − *Department of Physics, National Cheng Kung University, 701 Tainan, Taiwan;* orcid.org/0000-0002-7974-9852; Email: vokhuongdien@gmail.com

Ming-Fa Lin − *Department of Physics, National Cheng Kung University, 701 Tainan, Taiwan; Hierarchical Green-Energy Material (Hi-GEM) Research Center, National Cheng Kung University, 701 Tainan, Taiwan;* orcid.org/0000-0002-0531-2068; Email: mflin@mail.ncku.edu.tw

Author

Nguyen Thi Han − *Department of Physics, National Cheng Kung University, 701 Tainan, Taiwan*

Complete contact information is available at: https://pubs.acs.org/10.1021/acsomega.2c02088

Author Contributions

N.T.H. designed the study and wrote the manuscript. V.K.D. performed the simulations and analyzed the results. M.-F.L. supervised this work. All authors discussed the results and revised the manuscript.

Notes

The authors declare no competing financial interest.

https://doi.org/10.1021/acsomega.2c02088
ACS Omega 2022, 7, 25210−25218

■ ACKNOWLEDGMENTS

This work was financially supported by the Hierarchical Green-Energy Materials (Hi-GEM) Research Center from The Featured Areas Research Center Program within the framework of the Higher Education Sprout Project by the Ministry of Education (MOE) and the Ministry of Science and Technology (MOST 110-2634-F-006 -017) in Taiwan.

■ REFERENCES

(1) Sun, Y.; Zhang, W.; Chi, H.; Liu, Y.; Hou, C. L.; Fang, D. Recent development of graphene materials applied in polymer solar cell. *Renewable Sustainable Energy Rev.* **2015**, *43*, 973−980.
(2) Humada, A. M.; Hojabri, M.; Mekhilef, S.; Hamada, H. M. Solar cell parameters extraction based on single and double-diode models: A review. *Renewable Sustainable Energy Rev.* **2016**, *56*, 494−509.
(3) Lee, T. D.; Ebong, A. U. A review of thin film solar cell technologies and challenges. *Renewable Sustainable Energy Rev.* **2017**, *70*, 1286−1297.
(4) Nayak, P. K.; Mahesh, S.; Snaith, H. J.; Cahen, D. Photovoltaic solar cell technologies: analysing the state of the art. *Nat. Rev. Mater.* **2019**, *4*, 269−285.
(5) Jung, H. S.; Park, N.-G. Perovskite solar cells: from materials to devices. *Small* **2015**, *11*, 10−25.
(6) Yun, S.; Qin, Y.; Uhl, A. R.; Vlachopoulos, N.; Yin, M.; Li, D.; Han, X.; Hagfeldt, A. New-generation integrated devices based on dye-sensitized and perovskite solar cells. *Energy Environ. Sci.* **2018**, *11*, 476−526.
(7) Boix, P. P.; Nonomura, K.; Mathews, N.; Mhaisalkar, S. G. Current progress and future perspectives for organic/inorganic perovskite solar cells. *Mater. Today* **2014**, *17*, 16−23.
(8) Assadi, M. K.; Bakhoda, S.; Saidur, R.; Hanaei, H. Recent progress in perovskite solar cells. *Renewable Sustainable Energy Rev.* **2018**, *81*, 2812−2822.
(9) Correa-Baena, J.-P.; Saliba, M.; Buonassisi, T.; Grätzel, M.; Abate, A.; Tress, W.; Hagfeldt, A. Promises and challenges of perovskite solar cells. *Science* **2017**, *358*, 739−744.
(10) Hussain, I.; Tran, H. P.; Jaksik, J.; Moore, J.; Islam, N.; Uddin, M. J. Functional materials, device architecture, and flexibility of perovskite solar cell. *Emergent Mater.* **2018**, *1*, 133−154.
(11) Kim, H.-S.; Seo, J.-Y.; Park, N.-G. Material and device stability in perovskite solar cells. *ChemSusChem* **2016**, *9*, 2528−2540.
(12) Green, M. A.; Ho-Baillie, A.; Snaith, H. J. The emergence of perovskite solar cells. *Nat. Photonics* **2014**, *8*, 506−514.
(13) Ahmad, S.; Guo, X. Rapid development in two-dimensional layered perovskite materials and their application in solar cells. *Chin. Chem. Lett.* **2018**, *29*, 657−663.
(14) Wang, J.; Zhang, J.; Zhou, Y.; Liu, H.; Xue, Q.; Li, X.; Chueh, C.-C.; Yip, H.-L.; Zhu, Z.; Jen, A. K. Y. Highly efficient all-inorganic perovskite solar cells with suppressed non-radiative recombination by a Lewis base. *Nat. Commun.* **2020**, *11*, 1−9.
(15) Xiaohui, M.; Liqun, Y.; Shijian, Z.; Qilin, D.; Cong, C.; Hongwei, S. All-Inorganic Perovskite Solar Cells: Status and Future. *Prog. Chem.* **2020**, *32*, 1608.
(16) Jellicoe, T. C.; Richter, J. M.; Glass, H. F. J.; Tabachnyk, M.; Brady, R.; Dutton, S. E.; Rao, A.; Friend, R. H.; Credgington, D.; Greenham, N. C.; Böhm, M. L. Synthesis and optical properties of lead-free cesium tin halide perovskite nanocrystals. *J. Am. Chem. Soc.* **2016**, *138*, 2941−2944.
(17) Zhang, J.; Hodes, G.; Jin, Z.; Liu, S. All-inorganic CsPbX3 perovskite solar cells: progress and prospects. *Angew. Chem., Int. Ed.* **2019**, *58*, 15596−15618.
(18) Jiang, Y.; Yuan, J.; Ni, Y.; Yang, J.; Wang, Y.; Jiu, T.; Yuan, M.; Chen, J. Reduced-dimensional α-CsPbX3 perovskites for efficient and stable photovoltaics. *Joule* **2018**, *2*, 1356−1368.
(19) Men, L.; Rosales, B. A.; Gentry, N. E.; Cady, S. D.; Vela, J. Lead-Free Semiconductors: Soft Chemistry, Dimensionality Control, and Manganese-Doping of Germanium Halide Perovskites. *Chem-NanoMat* **2019**, *5*, 334−339.
(20) Dias, A. C.; Lima, M. P.; Da Silva, J. L. F. Role of Structural Phases and Octahedra Distortions in the Optoelectronic and Excitonic Properties of CsGeX3 (X= Cl, Br, I) Perovskites. *J. Phys. Chem. C* **2021**, *125*, 19142−19155.
(21) Roknuzzaman, M.; Ostrikov, K.; Wang, H.; Du, A.; Tesfamichael, T. Towards lead-free perovskite photovoltaics and optoelectronics by ab-initio simulations. *Sci. Rep.* **2017**, *7*, 1−8.
(22) Brik, M. G. Comparative first-principles calculations of electronic, optical and elastic anisotropy properties of CsXBr3 (X= Ca, Ge, Sn) crystals. *Solid State Commun.* **2011**, *151*, 1733−1738.
(23) Seo, D.-K.; Gupta, N.; Whangbo, M.-H.; Hillebrecht, H.; Thiele, G. Pressure-induced changes in the structure and band gap of CsGeX3 (X= Cl, Br) studied by electronic band structure calculations. *Inorg. Chem.* **1998**, *37*, 407−410.
(24) Huang, D.; Zhao, Y.-J.; Ju, Z.-P.; Gan, L.-Y.; Chen, X.-M.; Li, C.-S.; Yao, C.-m.; Guo, J. First-principles prediction of a promising p-type transparent conductive material CsGeCl3. *Appl. Phys. Express* **2014**, *7*, 041201.
(25) Erdinc, B.; Secuk, M. N.; Aycibin, M.; Gülebagan, S. E.; Dogan, E. K.; Akkus, H. Ab-initio study of CsGeCl3 compound in paraelectric and ferroelectric phases. *Ferroelectrics* **2016**, *494*, 138−149.
(26) Tang, L.-C.; Chang, Y.-C.; Huang, J.-Y.; Lee, M.-H.; Chang, C.-S. First principles calculations of linear and second-order optical responses in rhombohedrally distorted perovskite ternary halides, CsGeX3 (X= Cl, Br, and I). *Jpn. J. Appl. Phys.* **2009**, *48*, 112402.
(27) Körbel, S.; Marques, M. A.; Botti, S. Stability and electronic properties of new inorganic perovskites from high-throughput ab initio calculations. *J. Mater. Chem. C* **2016**, *4*, 3157−3167.
(28) Jaroenjittichai, A. P.; Laosiritaworn, Y. Band alignment of cesium-based halide perovskites. *Ceram. Int.* **2018**, *44*, S161−S163.
(29) Li, Y.; Li, Y. All-inorganic Perovskite Solar Cells. *Perovskite Sol. Cells* **2021**, *2021*, 175−221.
(30) Rezaei nik, Y.; Reyhani, A.; Farjami-Shayesteh, S.; Mortazavi, S. Z. Photocurrent enhancement of hybrid perovskite CsGeBr3 assisted two-dimensional WS2 nano-flakes based on electron-hole mobility improvement. *Opt. Mater.* **2021**, *112*, 110754.
(31) Schwarz, U.; Wagner, F.; Syassen, K.; Hillebrecht, H. Effect of pressure on the optical-absorption edges of CsGeBr 3 and CsGeCl 3. *Phys. Rev. B: Condens. Matter Mater. Phys.* **1996**, *53*, 12545.
(32) Chen, L.-J. Synthesis and optical properties of lead-free cesium germanium halide perovskite quantum rods. *RSC Adv.* **2018**, *8*, 18396−18399.
(33) Jong, U.-G.; Yu, C.-J.; Kye, Y.-H.; Choe, Y.-G.; Hao, W.; Li, S. First-principles study on structural, electronic, and optical properties of inorganic Ge-based halide perovskites. *Inorg. Chem.* **2019**, *58*, 4134−4140.
(34) Huang, L.-y.; Lambrecht, W. R. L. Electronic band structure trends of perovskite halides: Beyond Pb and Sn to Ge and Si. *Phys. Rev. B* **2016**, *93*, 195211.
(35) Han, N. T.; Dien, V. K.; Thuy Tran, N. T.; Nguyen, D. K.; Su, W.-P.; Lin, M.-F. First-principles studies of electronic properties in lithium metasilicate (Li 2 SiO 3). *RSC Adv.* **2020**, *10*, 24721−24729.
(36) Bouhmaidi, S.; Marjaoui, A.; Talbi, A.; Zanouni, M.; Nouneh, K.; Setti, L. A DFT study of electronic, optical and thermoelectric properties of Ge-halide perovskites CsGeX3 (X= F, Cl and Br). *Comput. Condens. Matter* **2022**, *31*, No. e00663.
(37) Xu, L.; Yang, M.; Wang, S. J.; Feng, Y. P. Electronic and optical properties of the monolayer group-IV monochalcogenides M X (M= Ge, Sn; X= S, Se, Te). *Phys. Rev. B* **2017**, *95*, 235434.
(38) Han, N. T.; Dien, V. K.; Lin, M.-F. Excitonic effects in the optical spectra of Li2SiO3 compound. *Sci. Rep.* **2021**, *11*, 1−10.
(39) Dien, V. K.; Pham, H. D.; Tran, N. T. T.; Han, N. T.; Huynh, T. M. D.; Nguyen, T. D. H.; Fa-Lin, M. Orbital-hybridization-created optical excitations in Li2GeO3. *Sci. Rep.* **2021**, *11*, 1−10.
(40) Dien, V. K.; Han, N. T.; Su, W.-P.; Lin, M.-F. Spin-dependent optical excitations in LiFeO2. *ACS Omega* **2021**, *6*, 25664−25671.
(41) Sun, G.; Kürti, J.; Rajczy, P.; Kertesz, M.; Hafner, J.; Kresse, G. Performance of the Vienna ab initio simulation package (VASP) in chemical applications. *J. Mol. Struct.: THEOCHEM* **2003**, *624*, 37−45.

https://doi.org/10.1021/acsomega.2c02088
ACS Omega 2022, 7, 25210−25218

(42) Perdew, J. P.; Burke, K.; Ernzerhof, M. Generalized gradient approximation made simple. *Phys. Rev. Lett.* **1996**, *77*, 3865.
(43) Kresse, G.; Joubert, D. From ultrasoft pseudopotentials to the projector augmented-wave method. *Phys. Rev. B: Condens. Matter Mater. Phys.* **1999**, *59*, 1758.
(44) Hine, N. D. M.; Robinson, M.; Haynes, P. D.; Skylaris, C.-K.; Payne, M. C.; Mostofi, A. A. Accurate ionic forces and geometry optimization in linear-scaling density-functional theory with local orbitals. *Phys. Rev. B: Condens. Matter Mater. Phys.* **2011**, *83*, 195102.
(45) Bruneval, F.; Botti, S.; Reining, L. Comment on "quantum confinement and electronic properties of silicon nanowires". *Phys. Rev. Lett.* **2005**, *94*, 219701.
(46) Wing, D.; Haber, J. B.; Noff, R.; Barker, B.; Egger, D. A.; Ramasubramaniam, A.; Louie, S. G.; Neaton, J. B.; Kronik, L. Comparing time-dependent density functional theory with many-body perturbation theory for semiconductors: Screened range-separated hybrids and the G W plus Bethe-Salpeter approach. *Phys. Rev. Mater.* **2019**, *3*, 064603.
(47) Schindlmayr, A.; Pollehn, T. J.; Godby, R. W. Spectra and total energies from self-consistent many-body perturbation theory. *Phys. Rev. B: Condens. Matter Mater. Phys.* **1998**, *58*, 12684.
(48) Mostofi, A. A.; Yates, J. R.; Lee, Y.-S.; Souza, I.; Vanderbilt, D.; Marzari, N. wannier90: A tool for obtaining maximally-localised Wannier functions. *Comput. Phys. Commun.* **2008**, *178*, 685−699.
(49) Pizzi, G.; Vitale, V.; Arita, R.; Blügel, S.; Freimuth, F.; Géranton, G.; Gibertini, M.; Gresch, D.; Johnson, C.; Koretsune, T.; Ibañez-Azpiroz, J.; Lee, H.; Lihm, J.-M.; Marchand, D.; Marrazzo, A.; Mokrousov, Y.; Mustafa, J. I.; Nohara, Y.; Nomura, Y.; Paulatto, L.; Poncé, S.; Ponweiser, T.; Qiao, J.; Thöle, F.; Tsirkin, S. S.; Wierzbowska, M.; Marzari, N.; Vanderbilt, D.; Souza, I.; Mostofi, A. A.; Yates, J. R. Wannier90 as a community code: new features and applications. *J. Phys.: Condens. Matter* **2020**, *32*, 165902.
(50) Crépieux, A.; Bruno, P. Theory of the anomalous Hall effect from the Kubo formula and the Dirac equation. *Phys. Rev. B: Condens. Matter Mater. Phys.* **2001**, *64*, 014416.
(51) Cutkosky, R. E. Solutions of a Bethe-Salpeter equation. *Phys. Rev.* **1954**, *96*, 1135.
(52) Hirata, S.; Head-Gordon, M. Time-dependent density functional theory within the Tamm−Dancoff approximation. *Chem. Phys. Lett.* **1999**, *314*, 291−299.
(53) Zhao, Z.; Li, Z.; Zou, Z. Electronic structure and optical properties of monoclinic clinobisvanite BiVO 4. *Phys. Chem. Chem. Phys.* **2011**, *13*, 4746−4753.
(54) Inoue, Y.; Kubokawa, T.; Sato, K. Photocatalytic activity of alkali-metal titanates combined with ruthenium in the decomposition of water. *J. Phys. Chem.* **1991**, *95*, 4059−4063.
(55) Bokdam, M.; Sander, T.; Stroppa, A.; Picozzi, S.; Sarma, D. D.; Franchini, C.; Kresse, G. Role of polar phonons in the photo excited state of metal halide perovskites. *Sci. Rep.* **2016**, *6*, 1−8.
(56) Xiang, G.; Wu, Y.; Zhang, M.; Leng, J.; Cheng, C.; Ma, H. Strain-induced bandgap engineering in CsGeX 3 (X= I, Br or Cl) perovskites: insights from first-principles calculations. *Phys. Chem. Chem. Phys.* **2022**, *24*, 5448−5454.
(57) Elsasser, W. M. Mean absorption and equivalent absorption coefficient of a band spectrum. *Phys. Rev.* **1938**, *54*, 126.
(58) Wooten, F.; Davis, S. P. Optical properties of solids. *Am. J. Phys.* **1973**, *41*, 939−940.
(59) Vrhel, M. J.; Gershon, R.; Iwan, L. S. Measurement and analysis of object reflectance spectra. *Color Res. Appl.* **1994**, *19*, 4−9.
(60) Thiele, G.; Rotter, H. W.; Schmidt, K. D. Kristallstrukturen und phasentransformationen von caesiumtrihalogenogermanaten (II) CsGeX3 (X= Cl, Br, I). *Z. Anorg. Allg. Chem.* **1987**, *545*, 148−156.
(61) Krishnamoorthy, T.; Ding, H.; Yan, C.; Leong, W. L.; Baikie, T.; Zhang, Z.; Sherburne, M.; Li, S.; Asta, M.; Mathews, N.; Mhaisalkar, S. G. Lead-free germanium iodide perovskite materials for photovoltaic applications. *J. Mater. Chem. A* **2015**, *3*, 23829−23832.

https://doi.org/10.1021/acsomega.2c02088
ACS Omega 2022, 7, 25210−25218